DOI: 10.1002/ejic.200900990

Spectroscopic and Computational Study of Ligand Photodissociation from [Ru(dipyrido[3,2-*a*:2′,3′-*c*]phenazine)(4-aminopyridine)$_4$]$^{2+}$

Tiziana Ruiu,[a] Claudio Garino,[a] Luca Salassa,[b] Ana M. Pizarro,[b] Carlo Nervi,[a] Roberto Gobetto,*[a] and Peter J. Sadler*[b]

Keywords: Photochemistry / Ruthenium / Density functional calculations / Dipyridophenazine / N ligands

The new complex [Ru(dppz)(4AP)$_4$]$^{2+}$ (**1**, in which dppz = dipyrido[3,2-*a*:2′,3′-*c*]phenazine and 4AP = 4-aminopyridine) has been synthesized, characterized and its photophysical and photochemical properties have been studied by combining spectroscopic and computational [DFT and time-dependent (TD) DFT] methods. Upon irradiation in aqueous solution, complex **1** selectively photoreleases one 4AP ligand and subsequently coordinates a water molecule to form [Ru(dppz)(4AP)$_3$(OH$_2$)]$^{2+}$.

Introduction

The release of coordinated ligands can be phototriggered at relatively low energy in transition-metal complexes due to the intrinsic nature of the metal–ligand bond. Several light-activated transition-metal complexes have been recently developed for in vitro applications such as "cage" metal complexes containing coordinated ligands with regulatory/biochemical function or, alternatively, metal complexes that, once irradiated, bind selectively to target biomolecules, thus performing their function as anticancer agents.[1–9]

Etchenique and co-workers[1] reported the complex [Ru(bpy)$_2$(4AP)$_2$]$^{2+}$ (bpy = 2,2′-bipyridine and 4AP = 4-aminopyridine), which releases the neuro-active ligand 4AP (inhibitor of voltage-gated K-channels) by irradiation with visible light ($\lambda > 480$ nm).

Strategies to deliver NO to biological targets have been extensively developed by Ford and others.[2] Such systems usually employ a precursor that displays relatively low thermal reactivity but is photochemically active towards the release of NO. For example, metal nitrosyl complexes such as the iron–sulfur–nitrosyl Roussin's cluster anions [Fe$_2$S$_2$(NO)$_4$]$^{2-}$ and [Fe$_4$S$_3$(NO)$_7$]$^-$ as well as metalloporphyrin nitrosyls, including ferriheme complexes and nitrosyl nitrito complexes of ruthenium porphyrins [Ru(Por)(ONO)(NO)] (in which Por indicates a porphyrin ligand), have been suggested as potential candidates.

A limited number of examples of metal-based chemotherapeutics that mimic cisplatin after light activation have appeared in the literature. In the majority of these metal complexes, ligand loss is promoted by excitation of a band in the ultraviolet type A (UVA) or visible region of the electronic absorption spectrum, and DNA-reactive aqua species are formed. Examples include *cis*-[Rh$_2$(μ-O$_2$CCH$_3$)$_2$(CH$_3$CN)$_6$]$^{2+}$, *cis*-[Ru(bpy)$_2$(NH$_3$)$_2$]$^{2+}$, *cis*-[Rh(bpy)$_2$(Cl)$_2$]$^{2+}$, [Ru(*p*-cym)(bpm)(py)]$^{2+}$ (*p*-cym = *p*-cymene, bpm = 2,2′-bipyrimidine and py = pyridine) and [Pt^{IV}(N$_3$)$_2$(OH)$_2$(X)(Y)] (N$_3$ = azide, X = NH$_3$ and Y = NH$_3$ or pyridine).[3–8]

The spatial and temporal control of the activation by the use of light radiation greatly increases the potential of such photodissociable molecules in disease treatment, thus giving the opportunity for specific tissues within an organism to be targeted.

To investigate the mechanisms of the light-induced ligand-substitution reactions, a thorough knowledge of the excited-state dynamics of photoactive metal complexes and the characterization of the photoproducts is needed. Density functional theory (DFT) and time-dependent density functional theory (TD-DFT) represent potent and efficient tools for excited-state characterization of transition-metal complexes.[10–14] The combination of computational methods and spectroscopic results can provide useful information for a full comprehension of the photochemistry of these systems.

In this paper, we report combined spectroscopic and computational (DFT and TD-DFT) studies on the ruthenium(II) complex [Ru(dppz)(4AP)$_4$](ClO$_4$)$_2$ [**1**(ClO$_4$)$_2$, in which dppz = dipyrido[3,2-*a*:2′,3′-*c*]phenazine and 4AP =

[a] Department of Chemistry IFM, University of Turin, Via P. Giuria 7, 10125 Torino, Italy
Fax: +39-11-6707855
E-mail: roberto.gobetto@unito.it
[b] Department of Chemistry, University of Warwick, Gibbet Hill Road, Coventry CV4 7AL, UK
Fax: +44-24-76523819
E-mail: p.j.sadler@warwick.ac.uk
Supporting information for this article is available on the WWW under http://dx.doi.org/10.1002/ejic.200900990.

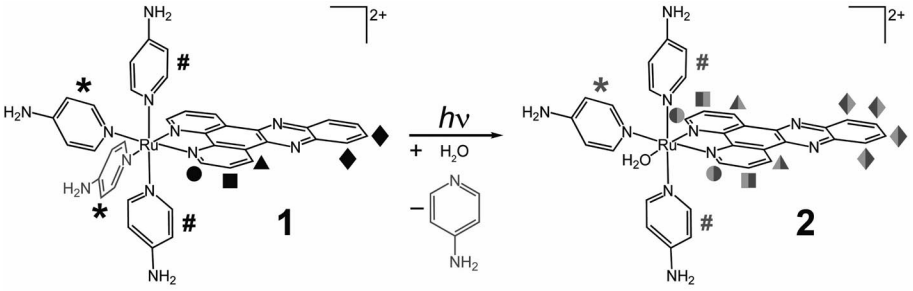

Figure 1. Schematic representation of the photodissociation of $[Ru(dppz)(4AP)_4]^{2+}$ (**1**) leading to the formation of $[Ru(dppz)(4AP)_3(OH_2)]^{2+}$ (**2**). Symbols refer to the labelling of specific protons or groups of protons.

4-aminopyridine], which contains the dppz ligand, known for its properties as a DNA intercalator.[15–22] Combining such properties with the photochemical features of $[Ru(N\text{-}N)(4AP)_4]^{2+}$ derivatives[23] can result in a novel mechanism of photoactivation. As summarized in Figure 1, photoactivation of **1** with visible light selectively induces the release of one equatorial (*trans* to dppz) 4AP ligand.

DFT analysis of singlet and triplet excited states provided useful insights into the photophysical and photochemical properties of **1**. The aim of this work is to establish a basis for detailed knowledge of the photochemistry of metal complexes, which represents a fundamental step in the design of molecules that are able to be efficiently photoactivated for applications in medicinal chemistry.

Results and Discussion

Synthesis and Structural Features

The complex $[Ru(dppz)(4AP)_4](ClO_4)_2$ [$\mathbf{1}(ClO_4)_2$] was synthesized according to a previously published procedure,[23] starting from [Ru(dppz)(*p*-cymene)Cl]Cl and 4-aminopyridine. The purple product was precipitated as a perchlorate salt; such a counterion was used to optimize (by minimizing water solubility) the reaction yield and the stability of **1** in the dark. The complex shows a one-electron metal-based reversible oxidation ($E_{1/2}$ = +0.355 V) and a one-electron ligand-based reversible reduction ($E_{1/2}$ = –1.416 V).

Geometry optimization of **1** in the gas phase was performed using both the B3LYP and PBE0 functionals, by employing the LanL2DZ basis set and effective core potential for the Ru atom, and either 6-31G** or 6-311G** basis sets for all other atoms. The main optimized geometrical parameters are reported in Table 1.

The four optimized structures obtained with different functionals and basis sets show that **1** has a pseudo-octahedral coordination structure. Ru–N bond lengths, obtained using different basis sets but with the same functional, have very close values, whereas little differences are found when comparing the two functionals B3LYP and PBE0. Unfortunately we were not able to get suitable crystals for X-ray diffraction analysis. After a search of the CCDC structural database we found examples of Ru–dppz complexes containing bipyridine; for example, the dimethyl-substituted dppz[24] and the 6,7-dicyano-substituted dppz.[25] In the former, the Ru–N(dppz), the equatorial Ru–N(bpy) and the axial Ru–N(bpy) bond lengths are in the range 2.04–2.05, 2.02–2.05 and 2.05–2.07 Å, respectively. In the 6,7-dicyano-substituted dppz the corresponding bond-length ranges are 2.07–2.10, 2.05–2.06 and 2.05–2.06 Å, respectively. The Ru–N(dppz) bond lengths obtained by our DFT calculations fall in the range observed experimentally, whereas the comparison between Ru–N(bpy) and Ru–N(4AP) bonds seems less important due to the intrinsic differences between the coordinated ligands. The PBE0 hybrid functional apparently shows a better performance over B3LYP. The reason is that in some cases the B3LYP exchange-correlation energy is developed and better parameterized to fit some sets of experimental data mostly concerning light elements of the first and second row.[26] In all optimized geometries, N–Ru–N angles are found to be very similar. The bite angle of the dppz ligand (N5–Ru–N6) is relatively small, close to 80°, whereas the angle between equatorial 4AP ligands (N3–Ru–N4) is approximately 91.6°. The axial 4AP ligands are slightly bent toward dppz, forming a N–Ru–N angle smaller than 180°.

Table 1. Selected bond lengths [Å] and angles [°] for optimized geometries of **1** (N1 and N2: axial 4AP; N3 and N4: equatorial 4AP; N5 and N6: dppz).

	B3LYP/ 6-31G**	B3LYP/ 6-311G**	PBE0/ 6-31G**	PBE0/ 6-311G**
Ru–N1	2.175	2.176	2.135	2.135
Ru–N2	2.172	2.173	2.136	2.135
Ru–N3	2.198	2.199	2.156	2.156
Ru–N4	2.197	2.199	2.156	2.156
Ru–N5	2.123	2.123	2.092	2.090
Ru–N6	2.120	2.119	2.092	2.090
N1–Ru–N2	178.98	178.94	178.95	179.06
N3–Ru–N4	91.57	91.57	91.62	91.68
N5–Ru–N6	78.49	78.34	79.09	78.99

Absorption and Emission Properties

Absorption and emission spectra of $\mathbf{1}(ClO_4)_2$ were recorded in aqueous solution and in dichloromethane. A small amount of DMSO (5%) was added to facilitate solubilization of the complex in the aqueous solution.

The absorption spectra recorded in the two solvents have similar features [Figure 2a and Table 2 (later)], showing a broad low-energy band, centred at 466 nm in H_2O and 463 nm in CH_2Cl_2. In dichloromethane two shoulders are also present at 530 nm (ε = 4794 $M^{-1}cm^{-1}$) and 600 nm (ε = 1690 $M^{-1}cm^{-1}$). The UV region of the spectrum shows a maximum around 280 nm (274 nm in H_2O, 281 nm in CH_2Cl_2) and three shoulders at 316, 355 and 375 nm in aqueous solution, and 320, 353 and 373 nm in dichloromethane. At higher energy a second intense band is also present at around 246 nm (247 nm in H_2O and 245 nm in CH_2Cl_2).

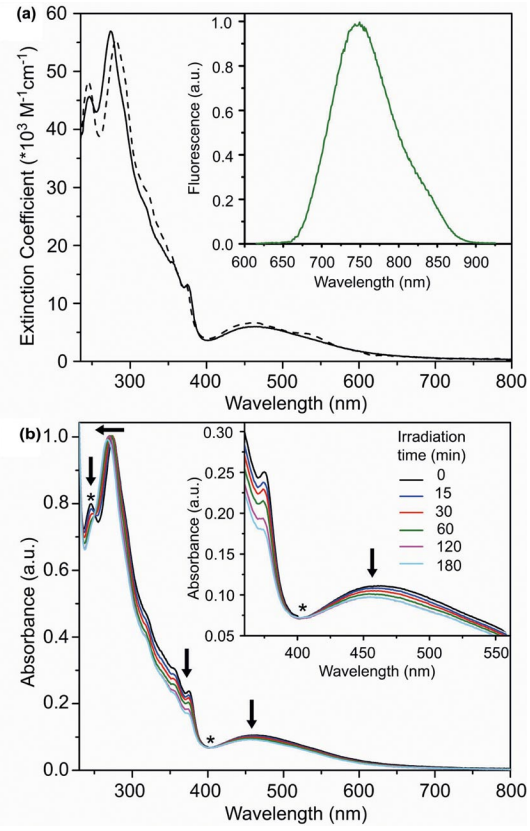

Figure 2. (a) UV/Vis absorption spectra of $\mathbf{1}(ClO_4)_2$ in aqueous solution (solid line) and CH_2Cl_2 (dashed line). Inset: emission spectra recorded in dichloromethane at room temperature. (b) Absorption spectrum of $\mathbf{1}(ClO_4)_2$ in aqueous solution, irradiated by 400–600 nm light (power 1 $J\,cm^{-2}\,h^{-1}$) for different time intervals (see legend in the inset). Inset: enlargement of the 360–560 nm region. Stars indicate isosbestic points.

As reported for other complexes containing the dppz ligand,[15,16] the emissive properties of **1** are extremely sensitive to the nature of the surrounding medium. Emission spectra of **1** were recorded at room temperature in deoxygenated solutions of several solvents. No luminescence was detected in solutions of **1** in water, acetonitrile or methanol; however, as expected, the emission of **1** significantly increased in dichloromethane. Upon excitation of the band centred at 463 nm, **1** gives an unstructured emission, centred at about 743 nm (13.5×10^3 cm^{-1}), not influenced by the concentration of oxygen (inset in Figure 2a). The measured lifetime at ambient temperature is 30 ns and the quantum yield is lower than 0.01 (approximated value due to the poor sensitivity of the detector above 700 nm). Short lifetimes have already been reported for ruthenium complexes of similar structures.[23,27–30]

Photodissociation Studies

The light-induced reaction of $\mathbf{1}(ClO_4)_2$ was monitored by ^1H NMR spectroscopy, UV/Vis spectroscopy and mass spectrometry. Water was employed in all experiments as the preferred solvent due to our interest in developing complexes that are able to be photoactivated for therapeutic applications (e.g., anticancer agents).[1,3,4,7,9,31–37] When irradiated with white light (400–600 nm, power 1 $J\,cm^{-2}\,h^{-1}$), the UV/Vis absorption spectrum of the complex slightly

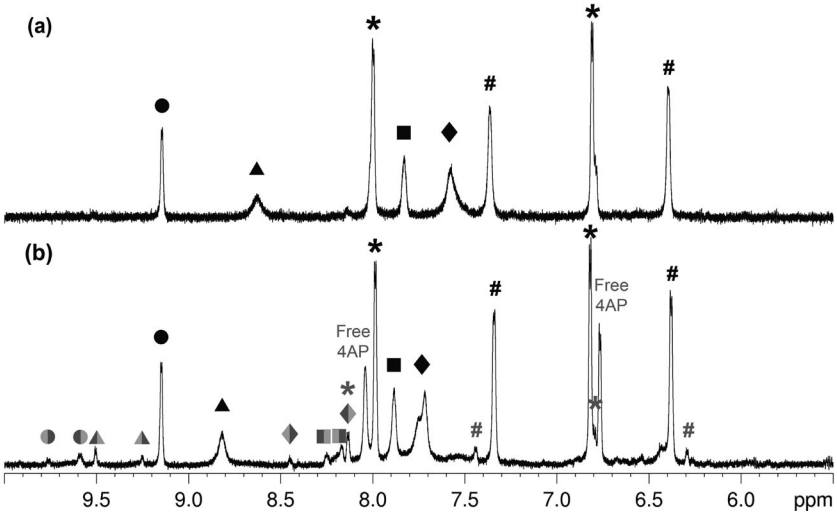

Figure 3. ^1H NMR spectrum of $\mathbf{1}(ClO_4)_2$ in D_2O/DMSO (95:5) (a) before, and (b) after 3 h of irradiation with white light (400–600 nm). For peak assignments see the labelling scheme in Figure 1.

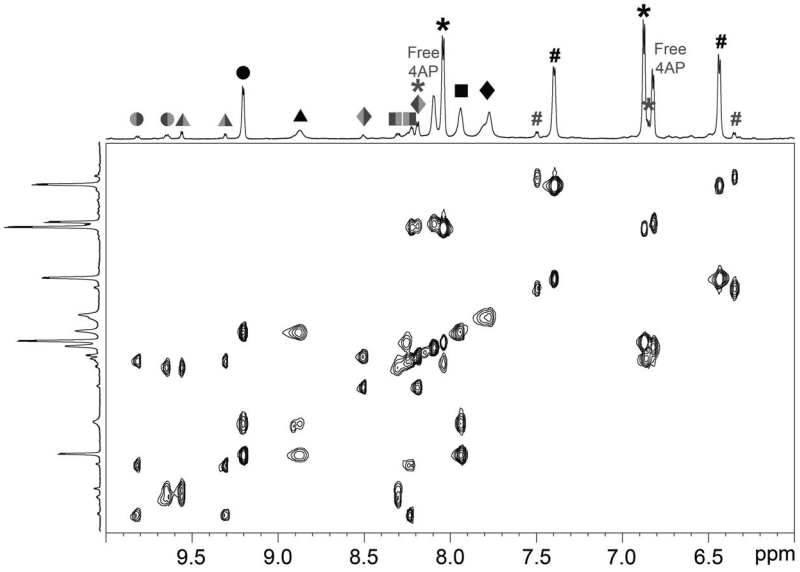

Figure 4. 2D ^{1}H–^{1}H TOCSY NMR spectrum of **1**$(ClO_4)_2$ in D_2O/DMSO (95:5). In the 1D spectrum, the peak assignment follows the labelling scheme shown in Figure 1.

changes over the time (Figure 2b). The intensity of the band around 460 nm progressively decreases, while the band at 274 nm is slightly blueshifted. The presence of two isosbestic points at 403 and 250 nm suggests the formation of a single photoproduct.

The ^{1}H NMR spectrum of **1** in the dark (Figure 3a) shows four peaks assignable to the five types of protons on the dppz ligand (one of these signals has double intensity) and four peaks with double intensity corresponding to the four sets of *ortho* and *meta* protons on both axial and equatorial 4AP ligands. ^{1}H–^{1}H COSY experiments and comparison with previous studies on similar complexes[23] allowed assignment of the doublets at δ = 6.83 and 8.00 ppm to the *ortho* and *meta* protons of the equatorial 4AP ligands (indicated by stars in Figure 3) and the peaks at δ = 6.40 and 7.36 ppm to the *ortho* and *meta* protons of the axial 4AP ligands (indicated by hashes in Figure 3).

Upon irradiation with white light, one equatorial 4AP ligand of the metal complex undergoes substitution by a water molecule, forming **2**, as shown in the ^{1}H NMR spectrum in Figure 3b. The proton signals relative to dppz become nonequivalent due to the loss of symmetry in complex **2**. ^{1}H–^{1}H TOCSY (Figure 4) and ^{1}H–^{1}H NOESY 2D NMR spectroscopy experiments confirm this assignment.

ESI mass spectra confirmed the formation of the aqua derivative after irradiation. Spectra of the solution before and after irradiation show three peaks assignable to the unreacted complex: the peak at *m*/*z* 380.10 corresponds to $\{Ru(dppz)(4AP)_4\}^{2+}$, that at *m*/*z* 333.08 to $\{Ru(dppz)(4AP)_3\}^{2+}$ and that at *m*/*z* 286.05 to $\{Ru(dppz)(4AP)_2\}^{2+}$. Irradiated solutions of **1**$(ClO_4)_2$ give two additional peaks, $\{[Ru(dppz)(4AP)_3(H_2O)]^{2+} - H\}^+$ at *m*/*z* 683.15 and $\{Ru(dppz)(4AP)_3(H_2O)\}^{2+}$ at *m*/*z* 342.08, which confirm the formation of photoproduct **2**.

Molecular Orbitals and Excited States Calculation

A series of DFT and TD-DFT calculations was performed to analyze the absorption and emission properties of **1** and to rationalize its photochemical behaviour. The modelling of **1** in protic (model **M1**, H_2O) and aprotic (model **M2**, CH_2Cl_2) solvents was performed using a dielectric continuum as an approximation to include the solvent effect [conductor-like polarizable continuum model (CPCM) method].[38–40] To improve the simulation of the aqueous environment, two explicit water molecules were added by means of hydrogen bonds to the nitrogen atoms of the phenazine portion of dppz (model **M3**).

The calculation of the electronic structure was preceded by the geometry optimization of the complex in the gas phase, performed with the B3LYP functional, and employing the LanL2DZ basis set and effective core potential for the Ru atom and the 6-311G** basis set for all other atoms (see the Exp. Section for details).

Orbital Analysis

An analysis of the more relevant frontier molecular orbitals, involved in the main electronic transitions, shows that in **M1**–**M3** the relative energy and shape of the MOs are very similar.

The three higher-energy occupied orbitals (HOMO, HOMO–1 and HOMO–2) are very close in energy and show a 65–70% metal character and a contribution of 11–17% from one or two 4AP ligands. The other occupied orbitals are separated from these HOMOs by 0.7 eV and have lower metal contributions. These orbitals play a marginal role in the electronic transitions, with the exception of HOMO–4, which involves mainly one axial 4AP and has a

limited metal character. HOMO–6 and HOMO–8 are dominated by the dppz contribution, which is higher than 93%.

The three unoccupied lower-energy orbitals LUMO, LUMO+1 and LUMO+2 are centred on the dppz ligand (contribution >95%). The other unoccupied orbitals are 1.25 eV above LUMO+2 and have a limited metal character and variable contributions from ligands. In the three models **M1**–**M3**, a set of antibonding LUMOs is present at higher energy, from LUMO+13 to LUMO+15. These orbitals are important for explaining the photodissociation process involving the metal complex, since they have an antibonding character toward the Ru–N bonds of both dppz and 4AP ligands.

UV/Vis Spectrum and Singlet Excited States

The nature of the electronic transitions responsible for the absorption bands was assigned using TD-DFT calculations. Eighty singlet excited states were computed both in H_2O (**M1**, **M3**) and CH_2Cl_2 (**M2**) by employing the gas-phase optimized geometry. The solvent effect was taken into account by using the CPCM method. In Table 2 and Figure 5 the experimental and calculated (**M1** and **M2**) absorption properties of **1** are compared. The singlet excited states obtained with the **M3** model do not differ significantly from **M1** and therefore are not discussed.

The experimental low-energy band centred around 460 nm in both H_2O and CH_2Cl_2 is slightly blueshifted by **M1** (452 nm) and **M2** (445 nm) calculations. Such a band is characterized by transitions in which the electron density migrates from a metal-centred orbital, with a small contribution from 4AP ligands, toward dppz. Moreover, a lower contribution to this band comes from a ^{1}MLCT transition (MLCT = metal-to-ligand charge transfer; **M1** 484 nm, **M2** 477 nm), in which an axial 4AP is significantly involved.

M2 explains the broadening of this band and the presence of shoulders at 530 and 600 nm observable in the experimental spectrum in CH_2Cl_2. These shoulders are due to other ^{1}MLCT (Ru→dppz) transitions.

The shoulder at 375 nm in H_2O and 373 nm in CH_2Cl_2 is correctly predicted by **M1** (372 nm) and **M2** (371 nm). **M2** assigns this band to a ^{1}MLCT having an electron-density migration from orbitals centred on the metal atom and on an axial 4AP to the dppz ligand; furthermore, in **M1** such ^{1}MLCT character is partially mixed with an intraligand dppz contribution.

The experimental maximum at 274 nm in H_2O is assigned by **M1** to an intense ^{1}LC transition calculated at 291 nm and localized on dppz. Another three strong transitions at 284, 298 and 299 nm (^{1}MLCT from Ru to all ligands) contribute to this band, together with several ^{1}MLCT transitions characterized by a lower oscillator strength.

Table 2. Experimental and calculated absorption properties for complex **1** in water and dichloromethane.

Solvent	λ_{abs} [nm]	ε [$M^{-1}cm^{-1}$]	Tr.[a]	$E_{calcd.}$ [eV] (λ_{abs} [nm])	f[b]	Composition	Character
H_2O (**M1**)	466	5997	8	2.74 (452)	0.1198	HOMO–1→LUMO+2 (53%) HOMO–2→LUMO+1 (19%)	MLCT (Ru→dppz)
	375[c]	13230	13	3.25 (382)	0.0211	HOMO–4→LUMO (94%)	MLCT (Ru/4AP$_{ax}$→dppz)
			16	3.34 (372)	0.0250	HOMO–6→LUMO (75%)	LC (dppz)
	355[c]	17060	19	3.52 (352)	0.0011	HOMO–3→LUMO+1 (93%)	LLCT (4APs→dppz)
	316[c]	27680	20	3.63 (342)	0.0748	HOMO–4→LUMO+1 (81%)	MLCT (Ru/4AP$_{ax}$→dppz)
			21	3.64 (340)	0.1880	HOMO–8→LUMO (68%)	LC (dppz)
	274	56920	46	4.14 (299)	0.3618	HOMO–1→LUMO+7 (24%) HOMO–2→LUMO+5 (–15%) HOMO–8→LUMO+1 (–10%)	MLCT (Ru→all ligands)
			50	4.17 (298)	0.1166	HOMO–2→LUMO+8 (22%) HOMO→LUMO+10 (14%) HOMO–8→LUMO+1 (–15%)	MLCT (Ru→4APs/dppz)
			57	4.26 (291)	0.8901	HOMO–6→LUMO+2 (53%) HOMO–8→LUMO (–12%)	mainly LC (dppz)
			64	4.36 (284)	0.1125	HOMO–2→LUMO+10 (63%)	MLCT (Ru→4APs)
	247	45670	77	4.74 (262)	0.4147	HOMO–13→LUMO+1 (52%)	mainly LC (dppz)
CH_2Cl_2 (**M2**)	463	6653	8	2.79 (445)	0.1176	HOMO–1→LUMO+2 (47%) HOMO→LUMO+2 (25%)	MLCT (Ru→dppz)
	373[c]	13240	15	3.33 (372)	0.0267	HOMO–6→LUMO (85%)	LC (dppz)
			16	3.34 (371)	0.0344	HOMO–4→LUMO (87%)	MLCT (Ru/4AP$_{ax}$→dppz)
	353[c]	18500	19	3.61 (344)	0.0597	HOMO–7→LUMO (77%)	MLCT (Ru/4AP$_{eq}$→dppz)
	320[c]	29610	21	3.67 (338)	0.1544	HOMO–8→LUMO (60%)	mainly LC (dppz)
	281	55520	46	4.16 (298)	0.6517	HOMO–2→LUMO+5 (25%) HOMO–2→LUMO+4 (10%)	MLCT (Ru→all ligands)
			49	4.18 (296)	0.2457	HOMO–2→LUMO+7 (32%)	MLCT (Ru→all ligands)
			55	4.24 (292)	0.4120	HOMO–6→LUMO+2 (28%) HOMO–2→LUMO+4 (16%) HOMO–8→LUMO (8%)	MLCT (Ru→all ligands)
			63	4.39 (282)	0.0944	HOMO–2→LUMO+10 (66%)	MLCT (Ru→4APs)
	245	48240	74	4.72 (263)	0.4972	HOMO–12→LUMO+1 (52%)	LC (dppz)/LLCT (4APs→dppz)

[a] Tr. indicates transition number as obtained in the TD-DFT calculation output. [b] f = oscillator strength. [c] Shoulders.

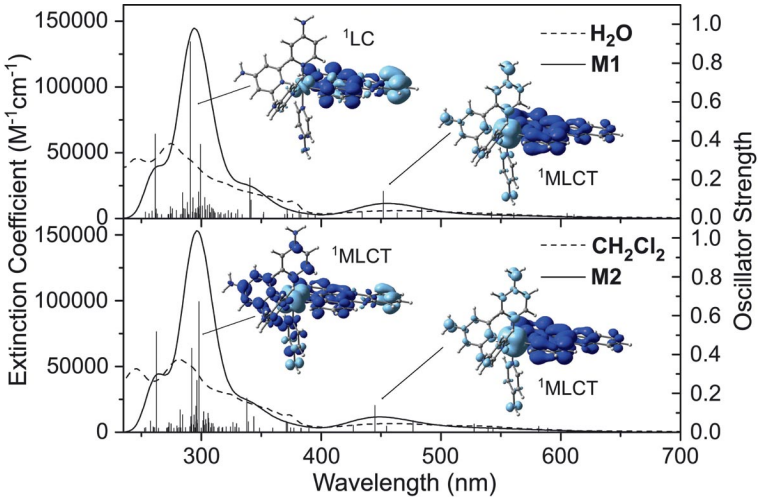

Figure 5. Calculated (**M1** and **M2**, solid lines) and experimental (dashed lines) UV/Vis absorption spectra of **1** in aqueous solution (top) and dichloromethane (bottom). Electronic transitions are represented as vertical bars with height equal to the oscillator strength (*f*) values. EDDMs (electron-density difference maps) of the foremost electronic transitions are also shown (light blue indicates a decrease in electron density, blue indicates an increase; isovalue = 0.001). Calculated spectra and EDDMs were obtained using the program GaussSum 1.05.[41]

In the case of CH_2Cl_2, **M2** assigns the experimental maximum centred at 281 nm to a series of ^{1}MLCT transitions calculated at 282, 292, 296 and 298 nm. In addition, several other ^{1}MLCTs with a low oscillator strength are contributing to this band.

The intense band at 247 nm in aqueous solution (**M1**, 262 nm) and 245 nm in dichloromethane (**M2**, 263 nm) can be assigned to a mixed ^{1}LC/^{1}LLCT transition involving mainly the dppz and the axial 4AP ligands.

Emission Properties and Triplet Excited States

Only in aprotic solvents (e.g., CH_2Cl_2) does **1** show an unstructured emission at 743 nm upon excitation of the MLCT band (463 nm). To study the nature of the emitting triplet state, we performed an unrestricted DFT [unrestricted Kohn–Sham formalism (UKS)] calculation to obtain the gas-phase structure of the lowest-lying triplet state (T_1) of the complex. The optimized geometry was used to estimate the emission energy using both TD-DFT and ΔSCF (SCF: self-consistent field) approaches (**M2**) by taking into account the solvent effect with the CPCM method (see the Exp. Section for details).[14,23,42–44]

The spin density of the lowest-lying triplet state, calculated with the UKS method as the difference between the α and β densities, was used to describe the nature of the T_1 state. The surface obtained in this way (Figure 6a) shows that T_1 has a ^{3}MLCT character (Ru/4AP$_{ax}$ → dppz), which involves the metal centre, the bidentate ligand dppz and one axial (ax) 4AP. This UKS result is in agreement with the TD-DFT calculation on triplet states, and in fact the EDDM relative to the lowest triplet (calculated at the triplet geometry) shows the same ^{3}MLCT character for the emissive state (Figure 6b).

The emission energy evaluated using the two approaches is in good agreement with the experimental data, although slightly different results are found from the two methods. ΔSCF underestimates the emission energy providing a value of 772 nm (13.0×10^3 cm^{-1}), whereas TD-DFT overestimates somewhat its value to 715 nm (14.0×10^3 cm^{-1}).

The **M1** and **M3** models show that in water the lowest-lying triplet spin density surface is identical to that obtained in dichloromethane. Nevertheless, such a triplet state has lower energy in **M1** and **M3** than in **M2**. Moreover, simulations in H_2O have a π–π* state lying close in energy to the lowest-lying triplet state (0.60 eV for **M1** and 0.72 eV for

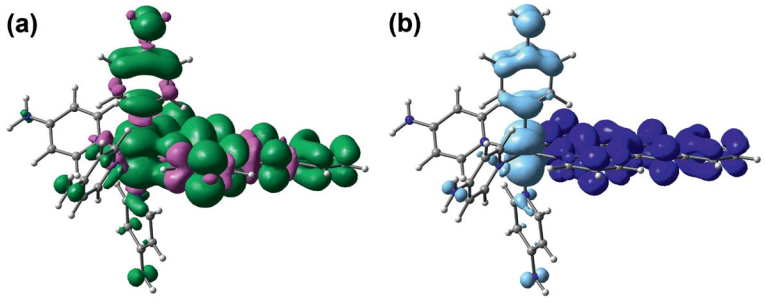

Figure 6. (a) Contour plot of the spin density of the lowest-lying triplet-state geometry of **1** in dichloromethane (isovalue = 0.0004). (b) EDDM relative to the first triplet transition (light blue indicates a decrease in electron density, whereas dark blue indicates an increase).

M3, instead of 1.08 eV for **M2**). Such a π–π* state resembles the dark state found for $[Ru(bpy)_2(dppz)]^{2+}$ by Batista and Martin[19] and its relative energy with respect to T_1 can account for the absence of emission in aqueous solution, although in all the other Ru–dppz systems studied computationally such a dark state is the lowest in energy.[18,20,45]

Photochemistry and DFT Calculations

When exposed to light, complex **1** releases one 4AP ligand. The presence of free 4AP was clearly visible in the ^1H NMR spectrum of a solution of **1** in D_2O (5% [D_6]-DMSO) exposed to white light (400–600 nm, power 1 $J\,cm^{-2}\,h^{-1}$), see Figures 3 and 4. ^1H–^1H TOCSY experiments confirmed that the metal complex undergoes substitution of one equatorial 4AP, *trans* to dppz, by a water molecule.

To identify the relevant excited electronic states responsible for the photodissociation of the 4AP ligand, and to confirm the results obtained spectroscopically, we analyzed the foremost frontier molecular orbitals involved in the main electronic transitions.

The set of two nearly degenerate antibonding LUMOs lying at higher energy (5.43 eV from the HOMO and 2.86 eV from the LUMO) is important for explaining the photodissociation process involving the metal complex. These orbitals, LUMO+14 and LUMO+15, have in fact an antibonding character in the Ru–N bonds of both dppz and 4AP ligands. In particular, LUMO+14 has a significant (47%) contribution from d metal orbitals and shows a σ-antibonding character along the Ru–N bonds, involving the two axial 4AP ligands (11%), one equatorial 4AP (7%) and a chelating N of dppz (34%). In LUMO+15, the metal d character is higher (55%) and the σ-antibonding character is found in the Ru–N bonds lying in the plane of dppz, involving the two equatorial 4AP ligands (16%) and the two chelating nitrogen atoms of dppz (24%).

The introduction of two water molecules interacting by means of hydrogen bonding with dppz (**M3**) does not significantly modify the model in which the molecule is embedded in the dielectric medium (**M1**). The relative energies and shapes of HOMOs are very similar to **M1**. The first three LUMOs (LUMO, LUMO+1 and LUMO+2) maintain the same shape, but are slightly lowered in energy due to the effect of the two water molecules bound to dppz. The other LUMOs are not shifted in energy, but their shape is in some cases different. LUMO+14 and LUMO+15 are very similar to the previous calculation; the bonding of the two water molecules does not change their energy and shape.

TD-DFT calculations in water (with or without hydrogen-bonded H_2O molecules) show that these antibonding MOs can be populated during low-energy electronic transitions, likely triggering the photodissociation of a 4AP ligand from the metal complex.

The photodissociation process can be explained by studying the nature of these dissociative excited states (Table 3).

Table 3. Calculated singlet and triplet transitions with dissociative character for **1** in water.

Solv.	Tr.[a]	$E_{calcd.}$ [eV] (λ_{abs} [nm])	f	Composition
H_2O (**M3**)	S_{12}	3.18 (390)	0.0007	HOMO–5→LUMO+2 (–32%) HOMO–1→LUMO+14 (32%)
	S_{13}	3.20 (387)	0.001	HOMO–5→LUMO (64%) HOMO–1→LUMO+14 (15%)
	S_{14}	3.24 (382)	0.001	HOMO–2→LUMO+15 (–25%) HOMO→LUMO+15 (25%)
	S_{16}	3.29 (372)	0.0025	HOMO–2→LUMO+14 (26%) HOMO–1→LUMO+15 (–16%) HOMO→LUMO+14 (17%)
	T_{14}	2.92 (423)	0.0	HOMO–2→LUMO+16 (16%) HOMO–1→LUMO+14 (–19%) HOMO–1→LUMO+16 (–31%)

[a] Tr. indicates transition number as obtained in the TD-DFT calculation output.

The absorption of near-UV/blue light (375–430 nm) promotes the population of singlet excited states (S_{12}, S_{13}, S_{14} and S_{16}), which have a dissociative character towards the Ru–N(4AP) bonds. These electronic transitions involve the σ-antibonding orbitals LUMO+14 and LUMO+15 (see Figures S1 and S2 in the Supporting Information). Analogous triplet excited states (T_{12} in **M1** and T_{14} in **M3**), with a dissociative character towards the Ru–N(4AP) bond, have similar energies and can be populated through intersystem crossing. Release of the 4AP ligand by photoexcitation can occur from these singlet/triplet excited states.

Conclusion

In this paper we have shown that the novel complex $[Ru(dppz)(4AP)_4]^{2+}$ (**1**) undergoes specific and selective photodissociation of one 4-aminopyridine (4AP) ligand. We have fully characterized the structure and the photophysical properties of **1** and identified the products of the light-induced reaction by NMR spectroscopy and mass spectrometry.

By employing DFT and TD-DFT calculations we have gained insights into the emission and photochemical behaviour of **1**.

Despite the finding that DFT can be successfully employed to predict the photochemistry of metal complexes, accurate descriptions of Ru–dppz-containing systems are still difficult to obtain, as shown before by several authors.[18–20,45] Nevertheless, the presence of singlet and triplet transitions involving σ-antibonding orbitals, such as LUMO+14 and LUMO+15, seems to be consistent with the observed photochemical activity.

Experimental Section

Materials and Reagents: All solvents in the synthetic procedures were of analytical/reagent grade and purified according to literature procedures.[46] Ruthenium(III) chloride hydrate was purchased

from Lancaster. The reagents 4-aminopyridine (4AP), 1,10-phenanthroline, 1,2-diaminobenzene, α-phellandrene, potassium bromide and sodium perchlorate were purchased from Aldrich and used without further purification. Dipyrido[3,2-*a*:2′,3′-*c*]phenazine (dppz) was synthesized according to a published procedure.[47]

NMR Spectroscopy: NMR spectra were recorded on a JEOL EX 400 spectrometer (^{1}H operating frequency 400 MHz) and on a Bruker DMX 600 spectrometer (^{1}H operating frequency 600 MHz). ^{1}H NMR spectroscopic signals were referenced to the residual solvent peak; for aqueous solutions, dioxane was added as an internal reference (δ = 3.75 ppm) and 5% deuterated DMSO was added to increase the solubility of the complex.

UV/Vis and Emission Spectroscopy: UV/Vis absorption spectra were measured with a double-beam Perkin–Elmer Lambda 20 UV/Vis spectrophotometer equipped with 1 cm quartz cell. Room-temperature emission spectra as well as luminescence lifetimes were obtained using a HORIBA Jobin Yvon IBH Fluorolog-TCSPC spectrofluorimeter. Luminescence quantum yields (ϕ) were determined using $[Ru(bpy)_3]Cl_2$ as standard (ϕ = 0.062).[48] Refractive index corrections were made to account for the different solvents used. Luminescence lifetimes were determined by time-correlated single-photon counting. Excitation with nanosecond pulses of 455 nm light (repetition rate 1 MHz) generated by a NanoLED pulsed diode was used for lifetime measurements. The emission data were collected using a spectral bandwidth of 10 nm. The data were collected into 2048 channels to 10000 counts in the peak channel. The sample was maintained at 20 °C in an automated sample chamber (F-3004 Peltier sample cooler from Horiba Jobin Yvon IBH) for ambient-temperature measurements. Emission decay data were analyzed using the software DAS6 (TCSPC decay analysis software). Decays were fit with reconvolution of the time-dependent profile of the light source. The best fit was assessed based on the parameter χ^2, which was close to 1.0, and the distribution of the weighted residual along the zero line.

High-Resolution Electrospray Mass Spectrometry: HRMS data were obtained on a Bruker MaXis electrospray ultra-high resolution tandem TOF (UHR-Qq-TOF) mass spectrometer. All the samples were analyzed by ESI(+) at 2 μL min^{-1}, nebulizer gas 0.4 bar, dry gas 4 L min^{-1} and dry temp. 180 °C, funnel RF 200 Vpp (RF: radio frequency; Vpp: peak-to-peak voltage), multiple RF 200, quadrupole ion energy 4 eV, collision cell 5 eV, ion cooler RF settings, ramp from 50 to 250 V. The *m*/*z* values reported are the strongest in the isotope envelope, and formulations were confirmed by matching isotope patterns with simulated ones generated with ISOTOPE.[49]

Electrochemical Measurements: Electrochemistry was carried out on samples in acetonitrile with 0.1 M tetrabutylammonium hexafluorophosphate ($TBAPF_6$) as supporting electrolyte, using a standard three-electrode cell configuration (glassy carbon working electrode, Pt counter electrode, 3 M KCl calomel reference electrode) and an Autolab PGSTAT302N electrochemical analyzer. All measurements were carried out in acetonitrile, distilled from calcium hydride just before use, under an Ar atmosphere. Ferrocene (Fc) was used as an internal standard, and potentials are reported against the Fc(0/+1) redox couple (measured $E_{1/2}$(0/+1) = 0.381 V).

Computational Details: All calculations were performed with the Gaussian 03 (G03) program,[50] by employing the DFT method with the B3LYP[51,52] functional. The LanL2DZ[53] basis set and effective core potential was employed for the Ru atom, whereas the 6-311G**[54] basis set was used for all other atoms. The ground-state geometry was optimized in the gas phase also with the PBE0[55,56] functionals. The lowest-lying triplet-state geometry was optimized in the gas phase using the unrestricted Kohn–Sham formalism (UKS). The nature of all stationary points was confirmed by normal-mode analysis. Electronic structures of singlet and triplet states were evaluated including the solvent effect by employing the CPCM[38–40] method, with water (models **M1** and **M3**) or dichloromethane (model **M2**) as solvent.

The UV/Vis spectra were calculated by TD-DFT[57,58] (80 singlet electronic transitions) including the solvent effect with the CPCM[38–40] method. The program GaussSum 1.05[41] was used to simulate the electronic spectra of the ruthenium complex and to visualize the singlet excited state transitions as EDDMs.[59,60]

The emission energy was evaluated in dichloromethane and water by the ΔSCF[10] and TD-DFT[61,62] approach, taking into account the solvent effect with the CPCM method. The ΔSCF approach calculates the vertical energy gap between the ground state (S_0) and the lowest-lying triplet state (T_1), both evaluated at the geometry optimized for T_1 and both computed using unrestricted wave functions (UKS). ΔSCF calculations yield the energy difference between the triplet excited states at their optimized geometries and the closed-shell ground state at the same geometry. This is a simple and reliable way to obtain emission energies. The TD-DFT approach calculates sixteen triplet excited states as electronic transitions from the ground state S_0, which was evaluated with T_1 optimized geometry. This TD-DFT calculation uses a restricted wave function. Triplet excited-state transitions were visualized as EDDMs by employing the program GaussSum 1.05.[41]

Synthesis of Complex 1: $[Ru(dppz)(4AP)_4](ClO_4)_2$ [**1**$(ClO_4)_2$] was obtained by using a slightly modified reported procedure.[23] [Ru(dppz)(*p*-cymene)Cl]Cl (455 mg, 0.773 mmol) and 4AP (733 mg, 7.79 mmol; ratio about 1:10) were heated at reflux in water for 5 d, stirring in an inert atmosphere and in the dark. The purple product was precipitated with sodium perchlorate and washed with aliquots of a saturated aqueous solution of sodium perchlorate, and then with water (670 mg, 90%).

Caution: *Perchlorate salts of metal complexes with organic ligands are potentially explosive. They should be handled with great care and in small quantities.*

^{1}H NMR (600 MHz, D_2O/[D_6]DMSO 5%, dioxane): δ = 6.40 (d, ^3J = 6.7 Hz, 4 H), 6.83 (d, ^3J = 6.6 Hz, 4 H), 7.36 (d, ^3J = 6.7 Hz, 4 H), 7.73 (2 H), 7.76 (2 H), 7.90 (2 H), 8.00 (d, ^3J = 6.6 Hz, 4 H), 8.83 (2 H), 9.16 (2 H) ppm. ^{1}H NMR (400 MHz, [D_6]acetone): δ = 6.08 (s, 4 H), 6.36 (d, ^3J = 7.2 Hz, 4 H), 6.44 (s, 4 H), 6.91 (d, ^3J = 7.0 Hz, 4 H), 7.36 (d, ^3J = 7.2 Hz, 4 H), 8.05 (d, ^3J = 7.0 Hz, 4 H), 8.17 (m, 2 H), 8.22 (dd, ^3J = 8.1 Hz, ^4J = 5.6 Hz, 2 H), 8.48 (m, 2 H), 9.33 (d, ^3J = 5.6 Hz, 2 H), 9.65 (d, ^3J = 8.1 Hz, 2 H) ppm. ^{13}C NMR (400 MHz, [D_6]acetone): δ = 110.7, 111.2, 126.8, 129.7, 130.5, 131.6, 132.3, 140.5, 142.8, 153.0, 154.7, 155.2, 155.3, 155.4, 155.5 ppm. ESI-MS: *m*/*z*: 380.10 [$M^+ - 2ClO_4^-$], 333.08 [$M^+ - 2ClO_4^- - 4AP$], 286.05 [$M^+ - 2ClO_4^- - 2(4AP)$]. Cyclic voltammetry (CH_3CN): $E_{1/2}$ = –1.416 V (one-electron ligand-based reduction); $E_{1/2}$ = +0.355 V (one-electron metal-based oxidation).

Supporting Information (see also the footnote on the first page of this article): Selected molecular orbitals for complex **1**.

Acknowledgments

C. G. thanks Regione Piemonte for financial support. L. S. was supported by the Marie Curie Intra European Fellowship 220281 PHOTORUACD within the 7th European Community Framework Programme. We also thank the Medical Research Council (MRC)

and Science City/European Regional Development Fund (ERDF)/ Advantage West Midlands for support, and Dr. Lijiang Song for technical MS advice.

[1] L. Zayat, C. Calero, P. Albores, L. Baraldo, R. Etchenique, *J. Am. Chem. Soc.* **2003**, *125*, 882–883.
[2] P. C. Ford, J. Bourassa, K. Miranda, B. Lee, I. Lorkovic, S. Boggs, S. Kudo, L. Laverman, *Coord. Chem. Rev.* **1998**, *171*, 185–202.
[3] D. A. Lutterman, P. K. L. Fu, C. Turro, *J. Am. Chem. Soc.* **2006**, *128*, 738–739.
[4] T. N. Singh, C. Turro, *Inorg. Chem.* **2004**, *43*, 7260–7262.
[5] D. Loganathan, J. H. Rodriguez, H. Morrison, *J. Am. Chem. Soc.* **2003**, *125*, 5640–5641.
[6] P. J. Bednarski, R. Grunert, M. Zielzki, A. Wellner, F. S. Mackay, P. J. Sadler, *Chem. Biol.* **2006**, *13*, 61–67.
[7] S. Betanzos-Lara, L. Salassa, A. Habtemariam, P. J. Sadler, *Chem. Commun.* **2009**, 6622–6624.
[8] F. S. Mackay, J. A. Woods, H. Moseley, J. Ferguson, A. Dawson, S. Parsons, P. J. Sadler, *Chem. Eur. J.* **2006**, *12*, 3155–3161.
[9] L. Zayat, M. Salierno, R. Etchenique, *Inorg. Chem.* **2006**, *45*, 1728–1731.
[10] A. Vlček, S. Záliš, *Coord. Chem. Rev.* **2007**, *251*, 258–287.
[11] F. De Angelis, S. Fantacci, A. Selloni, M. K. Nazeeruddin, M. Grätzel, *J. Am. Chem. Soc.* **2007**, *129*, 14156–14157.
[12] D. Di Censo, S. Fantacci, F. De Angelis, C. Klein, N. Evans, K. Kalyanasundaram, H. J. Bolink, M. Grätzel, M. K. Nazeeruddin, *Inorg. Chem.* **2008**, *47*, 980–989.
[13] A. Albertino, C. Garino, S. Ghiani, R. Gobetto, C. Nervi, L. Salassa, E. Rosenberg, A. Sharmin, G. Viscardi, R. Buscaino, G. Croce, M. Milanesio, *J. Organomet. Chem.* **2007**, *692*, 1377–1391.
[14] C. Garino, R. Gobetto, C. Nervi, L. Salassa, E. Rosenberg, J. B. A. Ross, X. Chu, K. I. Hardcastle, C. Sabatini, *Inorg. Chem.* **2007**, *46*, 8752–8762.
[15] A. E. Friedman, J. C. Chambron, J. P. Sauvage, N. J. Turro, J. K. Barton, *J. Am. Chem. Soc.* **1990**, *112*, 4960–4962.
[16] E. J. C. Olson, D. Hu, A. Hormann, A. M. Jonkman, M. R. Arkin, E. D. A. Stemp, J. K. Barton, P. F. Barbara, *J. Am. Chem. Soc.* **1997**, *119*, 11458–11467.
[17] F. Pierard, A. Kirsch-De Mesmaeker, *Inorg. Chem. Commun.* **2006**, *9*, 111–126.
[18] M. Atsumi, L. Gonzalez, C. Daniel, *J. Photochem. Photobiol. A: Chem.* **2007**, *190*, 310–320.
[19] E. R. Batista, R. L. Martin, *J. Phys. Chem. A* **2005**, *109*, 3128–3133.
[20] S. Fantacci, F. De Angelis, A. Sgamellotti, N. Re, *Chem. Phys. Lett.* **2004**, *396*, 43–48.
[21] S. Fantacci, F. De Angelis, A. Sgamellotti, A. Marrone, N. Re, *J. Am. Chem. Soc.* **2005**, *127*, 14144–14145.
[22] L. M. Chen, J. Liu, J. C. Chen, C. P. Tan, S. Shi, K. C. Zheng, L. N. Ji, *J. Inorg. Biochem.* **2008**, *102*, 330–341.
[23] L. Salassa, C. Garino, G. Salassa, C. Nervi, R. Gobetto, C. Lamberti, D. Gianolio, R. Bizzarri, P. J. Sadler, *Inorg. Chem.* **2009**, *48*, 1469–1481.
[24] N. Komatsuzaki, R. Katoh, Y. Himeda, H. Sugihara, H. Arakawa, K. Kasuga, *J. Chem. Soc., Dalton Trans.* **2000**, 3053–3054.
[25] J. Rusanova, S. Decurtins, E. Rusanov, H. Stoeckli-Evans, S. Delahaye, A. Hauser, *J. Chem. Soc., Dalton Trans.* **2002**, 4318–4320.
[26] V. Vetere, C. Adamo, P. Maldivi, *Chem. Phys. Lett.* **2000**, *325*, 99–105.
[27] J. F. Endicott, Y.-J. Chen, *Coord. Chem. Rev.* **2007**, *251*, 328–350.
[28] Y.-J. Chen, P. Xie, M. J. Heeg, J. F. Endicott, *Inorg. Chem.* **2006**, *45*, 6282–6297.
[29] P. Xie, Y.-J. Chen, M. J. Uddin, J. F. Endicott, *J. Phys. Chem. A* **2005**, *109*, 4671–4689.
[30] D. S. Seneviratne, M. J. Uddin, V. Swayambunathan, H. B. Schlegel, J. F. Endicott, *Inorg. Chem.* **2002**, *41*, 1502–1517.
[31] F. S. Mackay, J. A. Woods, P. Heringova, J. Kašpárková, A. M. Pizarro, S. A. Moggach, S. Parsons, V. Brabec, P. J. Sadler, *Proc. Natl. Acad. Sci. USA* **2007**, *104*, 20743–20748.
[32] S. Le Gac, S. Rickling, P. Gerbaux, E. Defrancq, C. Moucheron, A. Kirsch-De Mesmaeker, *Angew. Chem. Int. Ed.* **2009**, *48*, 1122–1125.
[33] A. K. Patra, T. Bhowmick, S. Roy, S. Ramakumar, A. R. Chakravarty, *Inorg. Chem.* **2009**, *48*, 2932–2943.
[34] P. C. Ford, *Acc. Chem. Res.* **2008**, *41*, 190–200.
[35] E. J. Merino, J. K. Barton, *Biochemistry* **2008**, *47*, 1511–1517.
[36] S. W. Magennis, A. Habtemariam, O. Novakova, J. B. Henry, S. Meier, S. Parsons, I. D. H. Oswald, V. Brabec, P. J. Sadler, *Inorg. Chem.* **2007**, *46*, 5059–5068.
[37] R. E. Mahnken, M. A. Billadeau, E. P. Nikonowicz, H. Morrison, *J. Am. Chem. Soc.* **1992**, *114*, 9253–9265.
[38] V. Barone, M. Cossi, *J. Phys. Chem. A* **1998**, *102*, 1995–2001.
[39] M. Cossi, V. Barone, *J. Chem. Phys.* **2001**, *115*, 4708–4717.
[40] M. Cossi, N. Rega, G. Scalmani, V. Barone, *J. Comput. Chem.* **2003**, *24*, 669–681.
[41] N. M. O'Boyle, J. G. Vos, *GaussSum 1.0*, **2005**, Dublin City University; see also http://gausssum.sourceforge.net.
[42] L. Salassa, C. Garino, A. Albertino, G. Volpi, C. Nervi, R. Gobetto, K. I. Hardcastle, *Organometallics* **2008**, *27*, 1427–1435.
[43] C. Garino, T. Ruiu, L. Salassa, A. Albertino, G. Volpi, C. Nervi, R. Gobetto, K. I. Hardcastle, *Eur. J. Inorg. Chem.* **2008**, 3587–3591.
[44] L. Salassa, C. Garino, G. Salassa, R. Gobetto, C. Nervi, *J. Am. Chem. Soc.* **2008**, *130*, 9590–9597.
[45] G. Pourtois, D. Beljonne, C. Moucheron, S. Schumm, A. Kirsch-De Mesmaeker, R. Lazzaroni, J. L. Bredas, *J. Am. Chem. Soc.* **2004**, *126*, 683–692.
[46] W. L. F. Amarengo, D. D. Perrin, *Purification of Laboratory Chemicals*, 4th ed., Butterworth-Heinemann, Oxford, **1996**.
[47] M. Yamada, Y. Tanaka, Y. Yoshimoto, *Bull. Chem. Soc. Jpn.* **1992**, *65*, 1006–1011.
[48] A. Juris, V. Balzani, F. Barigelletti, S. Campagna, P. Belser, A. Von Zelewsky, *Coord. Chem. Rev.* **1988**, *84*, 85–277.
[49] L. J. Arnold, *J. Chem. Educ.* **1992**, *69*, 811.
[50] M. J. Frisch, G. W. Trucks, H. B. Schlegel, G. E. Scuseria, M. A. Robb, J. R. Cheeseman, J. A. Montgomery Jr., T. Vreven, K. N. Kudin, J. C. Burant, J. M. Millam, S. S. Iyengar, J. Tomasi, V. Barone, B. Mennucci, M. Cossi, G. Scalmani, N. Rega, G. A. Petersson, H. Nakatsuji, M. Hada, M. Ehara, K. Toyota, R. Fukuda, J. Hasegawa, M. Ishida, T. Nakajima, Y. Honda, O. Kitao, H. Nakai, M. Klene, X. Li, J. E. Knox, H. P. Hratchian, J. B. Cross, C. Adamo, J. Jaramillo, R. Gomperts, R. E. Stratmann, O. Yazyev, A. J. Austin, R. Cammi, C. Pomelli, J. W. Ochterski, P. Y. Ayala, K. Morokuma, G. A. Voth, P. Salvador, J. J. Dannenberg, V. G. Zakrzewski, S. Dapprich, A. D. Daniels, M. C. Strain, O. Farkas, D. K. Malick, A. D. Rabuck, K. Raghavachari, J. B. Foresman, J. V. Ortiz, Q. Cui, A. G. Baboul, S. Clifford, J. Cioslowski, B. B. Stefanov, G. Liu, A. Liashenko, P. Piskorz, I. Komaromi, R. L. Martin, D. J. Fox, T. Keith, M. A. Al-Laham, C. Y. Peng, A. Nanayakkara, M. Challacombe, P. M. W. Gill, B. Johnson, W. Chen, M. W. Wong, C. Gonzalez, and J. A. Pople, *Gaussian 03*, Revision D.01, Gaussian, Inc., Wallingford, CT, **2004**.
[51] A. D. Becke, *J. Chem. Phys.* **1993**, *98*, 5648–5652.
[52] C. Lee, W. Yang, R. G. Parr, *Phys. Rev. B* **1988**, *37*, 785–789.
[53] P. J. Hay, W. R. Wadt, *J. Chem. Phys.* **1985**, *82*, 270–283.
[54] A. D. McLean, G. S. Chandler, *J. Chem. Phys.* **1980**, *72*, 5639–5648.
[55] C. Adamo, V. Barone, *J. Chem. Phys.* **1999**, *110*, 6158–6170.
[56] C. Adamo, G. E. Scuseria, V. Barone, *J. Chem. Phys.* **1999**, *111*, 2889–2899.
[57] M. E. Casida, C. Jamorski, K. C. Casida, D. R. Salahub, *J. Chem. Phys.* **1998**, *108*, 4439–4449.

[58] R. E. Stratmann, G. E. Scuseria, M. J. Frisch, *J. Chem. Phys.* **1998**, *109*, 8218–8224.
[59] M. Head-Gordon, A. M. Grana, D. Maurice, C. A. White, *J. Phys. Chem.* **1995**, *99*, 14261–14270.
[60] W. R. Browne, N. M. O'Boyle, J. J. McGarvey, J. G. Vos, *Chem. Soc. Rev.* **2005**, *34*, 641–663.
[61] S. R. Stoyanov, J. M. Villegas, A. J. Cruz, L. L. Lockyear, J. H. Reibenspies, P. D. Rillema, *J. Chem. Theory Comput.* **2005**, *1*, 95–106.
[62] J. M. Villegas, S. R. Stoyanov, W. Huang, P. D. Rillema, *Inorg. Chem.* **2005**, *44*, 2297–2309.

Received: October 9, 2009
Published Online: February 8, 2010

